SLAC-PUB-2452
January 1980
(T)

AZIMUTHAL CORRELATIONS IN BRANCH CUT CONTRIBUTIONS TO $\pi^- p \to \pi^0 n$ SCATTERING*

R. W. B. Ardill
Royal Holloway College
Englefield Green, Surrey TW20 OEX, UK

Peter Koehler
Stanford Linear Accelerator Center, Stanford University

and

K. J. M. Moriarty
Royal Holloway College
Englefield Green, Surrey TW20 OEX, UK

ABSTRACT

We recommend a new recipe for calculating cut corrections by introducing azimuthal correlations between the conventional Pomeron and the regular Reggeon. This procedure is suggested within the context of the Reggeon calculus and amounts to a more general parameterization of the vertices of the theory than has been used so far. We apply Gribov's Reggeon diagram technique to the concrete case of pion-nucleon charge exchange between 6 GeV/c and Fermilab energies. We investigate how sensitive the helicity amplitudes are to a specific choice of the vertices. The vertices we have chosen reverse the counter-clockwise rotation of the non-flip rho pole. This results in the correct phase behavior of vector and tensor exchanges obviating the need to introduce a complicated Pomeron or Regge-Regge cuts.

Submitted to Nuovo Cimento Letters

---

* Work supported in part by the Department of Energy under contract number DE-AC03-76SF00515 and in part by NATO Fellowship.

I. Introduction

A simple and unique description of the phase and energy behavior of the rho exchange has not so far been achieved. A great number of cut modifying devices have been suggested ([1]). In this paper we approach the problem from a different standpoint, by proposing to calculate cut corrections by introducing azimuthal correlations between the Pomeron and the Reggeon. The Pomeron remains a simple pole with intercept exactly at 1.0 and a small slope of 0.3 $[(\text{GeV/c})^{-2}]$ as indicated by the ISR data. The Reggeon has a simple and smooth residue and its trajectory chooses sense. There are no boost factors enhancing the strength of the cut. Our method of calculating the cut modification relies entirely on the correlation kernel, which is purely real so as not to violate the analytic properties of the amplitudes. By introducing the correlation kernel we get a more general parameterization of the Gribov vertices than previously obtained ([2]). In terms of the Reggeon calculus the Gribov vertices are related to the Reggeon-particle scattering amplitudes. The absorption model is limited to the elastic pole exchange, whereas the correlation kernel takes account of the inelastic intermediate states. One may be able to constrain the correlation parameter by considering the Gribov vertices as form factors within the framework of the non-relativistic harmonic oscillator quark model. Here the absorption model would correspond to the ground state of the oscillator whereas the correlation kernel would allow for the nth level excitation relating its parameter to the oscillator length. Thus the radii of the Regge vertices and the correlation parameters are bound up in the effective interaction size.

([1]) A. C. Irving and R. P. Worden, Phys. Rep. 34, 117 (1977).
([2]) K. A. Ter-Matirosyan, Sov. J. Nucl. Phys. 10, 600 (1970); V. Yu Glebov, A. B. Kaidalov, S. T. Sukhorukov and K. A. Ter-Matirosyan, Sov. J. Nucl. Phys. 10, 609 (1970).

Correct cut models have to rotate the helicity nonflip amplitude clockwise ([3]). To achieve this it is only the ratio of Pomeron trajectory to effective interaction size which has to be large by comparison to that of the absorption model. It is not therefore necessary to give the Pomeron a substantially large real part or to invoke Regge-Regge cuts. It is enough to reduce the effective interaction size, and this we accomplish through taking care of the mutual orientation of the transverse momenta between the Pomeron pole and the regular Reggeon. We introduce logs dependences into the correlation parameters. This ensures a stable phase against large variations in energy, and also an improved, although not totally satisfactory, behavior of the differential cross section for FNAL energies ([4]).

II. Formalism

Our correlation modified cut stands effectively for Gribov's full double scattering amplitude ([5]):

$$M_{ab}^{(2)}(s,\underline{k}) = \frac{i}{\pi}\int_{-\infty}^{\infty} N(\underline{k}_a,\underline{k}_b,\underline{k},s)\,\delta^2(\underline{k}_a+\underline{k}_b-\underline{k})\,d^2\underline{k}_a\,d^2\underline{k}_b\,\eta_a\eta_b\,(s/s_o)^{\alpha_a(\underline{k}_a)+\alpha_b(\underline{k}_b)-2}$$

$$= \frac{i}{\pi}\int_{s_1 t}^{\infty}\frac{s_o\,ds_1}{\pi s_1}\int_{s_2 t}^{\infty}\frac{s_o\,ds_2}{\pi s_2}\int_{-\infty}^{\infty}\delta^2(\underline{k}_a+\underline{k}_b-\underline{k})\,d^2\underline{k}_a\,d^2\underline{k}_b$$

$$\cdot\ \mathrm{disc}\,F_1(\underline{k}_a,\underline{k}_b,\underline{k},s_1)\,\mathrm{disc}\,F_2(\underline{k}_a,\underline{k}_b,\underline{k},s_2)$$

$$\cdot\ \eta_a(\underline{k}_a)\,\eta_b(\underline{k}_b)\,(s/s_o)^{\alpha_a(\underline{k}_a)+\alpha_b(\underline{k}_b)-2}\ .$$

([3]) I. Ambats et al., Phys. Rev. D9, 1179 (1974).
([4]) A. V. Barnes et al., Phys. Rev. Lett. 37, 76 (1976).
([5]) K. A. Ter-Matirosyan, Sov. J. Nucl. Phys. 10, 715 (1970).

$\underline{k}_a$ and $\underline{k}_b$ with $k^2_{a,b} = |t_{a,b}|^2 = -t_{a,b}$ are the two-dimensional Reggeon momenta and $k^2 = (\underline{k}_a + \underline{k}_b)^2 = |t|$ is the total momentum transfer. The linear Reggeon trajectories are $\alpha_{a,b} = \alpha_{a,b}(0) - \alpha'_{a,b}k^2$. The energy scale is set $s_0 = 1$ GeV. η_a, η_b are the signature factors:

$$\eta_{a,b}(\underline{k}_{a,b}) = i\sigma_{a,b} \frac{\exp\left[i\frac{\pi}{2}\left(\frac{\sigma_{a,b}+1}{2} - \alpha_{a,b}(\underline{k}_{a,b})\right)\right]}{\cos\frac{\pi}{2}\left(\frac{\sigma_a+1}{2} - \alpha_{a,b}(\underline{k}_{a,b})\right)},$$

where $\sigma_{a,b} = \pm 1$.

The Gribov vertex N factorizes into $N_1 \cdot N_2$. These are the absorptive parts of the Reggeon-particle scattering amplitudes F_1 and F_2.

$$N_{1,2} = \int_{-\infty}^{\infty} F_{1,2}(\underline{k}_a,\underline{k}_b,\underline{k},s_{1,2}) \frac{ds_{1,2}}{2\pi i s_{1,2}} = \int_{s^t_{1,2}}^{\infty} \text{disc } F_{1,2}(\underline{k}_a,\underline{k}_b,\underline{k},s_{1,2}) \frac{ds_{1,2}}{\pi s_{1,2}}$$

where $s_{1,2}$ are the subenergies and $s^t_{1,2}$ the threshhold values. The two-body amplitude is given by Fig. 1. The subenergy planes s_1 and s_2 are divided into low and high mass regions such that $s_{1,2} < M^2$ and $s_{1,2} > M^2$, respectively. A special low mass unenhanced diagram where $s_1 < M^2$ and $s_2 < M^2$ is Gribov's high-energy approximation of the Mandelstam cut is shown in Fig. 2a and its eikonal in Fig. 2b. In our phase correction of $\pi^- p \to \pi^0 n$ we rely entirely on the non-planarity of such diagrams. With the high-mass region taking on its Reggeon behavior the full amplitude splits into four parts (Fig. 3). These are unenhanced (Fig. 3a),

semi-enhanced (Figs. 3b, 3c) and fully-enhanced diagrams (Fig. 3d). Here the low-mass and the triple- Reggeon couplings are depicted as non-planar.

Our two-body cut amplitude takes account of low and high-mass inelastic-intermediate states in the vertex N of Gribov's full double-scattering amplitude. The traditional eikonal or absorption model is based on a Gaussian form of the Gribov vertex $N(\underline{k}_a, \underline{k}_b)$ and does not allow for any intermediate states except the elastic one (Fig. 4a). The quasi-eikonal model allows for the formation of low-mass showers in the intermediate states after each rescattering (Fig. 4b). The showers enhance the cut strength for elastic scattering at forward direction by a constant factor. The phase and energy behavior of $\pi^- p \to \pi^0 n$, however, suggests a more subtle parameterization of N. N has to depend on the angle between $\underline{k}_a$ and $\underline{k}_b$. Since the high-mass peripheral nonelastic intermediate states are Regge-approximated, N also has to depend on s. This leads to the diagrams in Figs. 2,3 where the non-planar low-mass and triple-Regge couplings are indicated. We have parameterized $N(\underline{k}_a, \underline{k}_b, \underline{k}, s)$ for $\pi^- p \to \pi^0 n$ such that it describes the data satisfactorily and does not violate theoretical principles. The phenomenology of the Gribov vertex should then be related to the diagrams of Fig. 3.

The sum of these diagrams gives the cut a pole-like shrinkage at high energy, with the enhanced diagrams b, c and d at rising energies taking the lead over the unenhanced diagram a. Thus, the helicity Gribov vertex $N^{0,1}$ is parameterized

(upper indices o and 1 indicate nonflip and flip respectively) for the helicity nonflip as:

$$N^{o}(\underline{k}_a,\underline{k}_b,\underline{k},s) =$$

$$\beta_\rho^{o}(s)\beta_p^{o}(s) \quad \exp\left[-(c^{o}(s)-\tilde{c}^{o}(s)k^2)\ (\underline{k}_1-\underline{k}_2)^2 - \lambda_\rho^{o}(s)k_1^2 - \lambda_p^{o}(s)k_2^2\right] ,$$

and for the helicity flip:

$$N^{1}(\underline{k}_a,\underline{k}_b,\underline{k},s) =$$

$$\beta_\rho^{1}(s)\beta_p^{o}(s) \quad \exp\left[-(c^{1}(s)-\tilde{c}^{1}(s)k^2)\ (\underline{k}_1-\underline{k}_2)^2 - \lambda_\rho^{1}(s)k_1^2 - \lambda_p^{o}(s)k_2^2\right] ,$$

where $\quad c^{o,1}(s) = c_1^{o,1} + c_2^{o,1}\ \ln s \quad ,$

and $\quad \tilde{c}^{o,1}(s) = \tilde{c}_1^{o,1} + \tilde{c}_2^{o,1}\ (\ln s)^{-1} \quad .$

The ρ chooses sense, i.e., the flip vanishes at $\alpha_\rho = 0$.

m_N is the nucleon mass and ϕ_1 is the phase of the Reggeon momentum $\underline{k}_1$ in the following expression.

For the Reggeon we write:

$$M_\rho^{o}(s,k_1^2) = \beta_\rho^{o}(s) \quad \exp\left[\frac{i\pi}{2}\ (1-\alpha_\rho(0)) - \lambda_\rho^{o}(s)k_1^2\right] \quad ,$$

$$M_\rho^{1}(s,k_1^2) = \frac{\alpha_\rho}{2m_N}\ |\underline{k}_1|\ \exp\left[i\phi_1\right]\beta_\rho^{1}(s) \quad \exp\left[\frac{i\pi}{2}\ (1-\alpha_\rho(0)) - \lambda_\rho^{1}(s)\ k_1^2\right] ,$$

and for the Pomeron:

$$M_p^{o}(s,k_2^2) = i\beta_p^{o}(s) \quad \exp\left[-\lambda_p^{o}(s)k_2^2\right] \quad ,$$

which is s-channel conserving.

The Regge and Pomeron vertices are Gaussian:

$$\beta^{o,1}_{\rho,p}(s) = \hat{\beta}^{o,1}_{\rho,p}\ s^{\alpha_{\rho,p}(0)-1} \quad ,$$

$$\lambda^{o,1}_{\rho,p}(s) = \hat{\lambda}^{o,1}_{\rho,p} + \alpha'_{\rho,p}\ \ln s - \frac{i\pi}{2}\alpha'_{\rho,p} \quad .$$

The Pomeron is purely imaginary at $t = 0$ with our normalization such that the optical theorem reads:

$$\sigma_{tot} = 4\sqrt{\pi}\ \mathrm{Im}\ {}^{o}M^{o}(s,k^2 = 0) \quad .$$

We can now write the Gribov cut in terms of the traditional cut modified by a correlation kernel K:

$$M^{o,1}_{\rho\times p}(k^2,s) = \frac{i}{\pi^{3/2}}\int_{-\infty}^{\infty} M^{o,1}_{\rho}(k_1^2,s)K^{o,1}(\underline{k}_1,\underline{k}_2,\underline{k},s)M^{o,1}_{p}(k_2^2,s)\delta^2(\underline{k}-\underline{k}_1-\underline{k}_2)d^2\underline{k}_1 d^2\underline{k}_2 ,$$

where $K^{o,1}(\underline{k}_1,\underline{k}_2,\underline{k},s) =$

$$\exp -\left[c_1^{o,1} + c_2^{o,1}\ \ln s - (\tilde{c}_1^{o,1} + \tilde{c}_2^{o,1}/\ln s)\ k^2\right]\ (\underline{k}_1 - \underline{k}_2)^2 \quad .$$

The evaluation of the correlation-modified Gribov integral leads to a cut expression which is much different in its s and $|t|$ dependence by comparison with the canonical absorption cut. We write down explicitly

the helicity-nonflip correlation modified cut:

$$M^{o}_{\rho xP}(\underline{k},s) = \frac{\beta^{o}_{\rho}(s)\,\beta^{o}_{P}(s)\,\exp\left[i\frac{\pi}{2}(1-\alpha_{\rho}(o))+i\pi\right]}{2\sqrt{\pi}\left(\lambda^{o}_{\rho}(s)+4c^{o}(s)+4\tilde{c}^{o}(s)|t|+\lambda^{o}_{P}(s)\right)}$$

$$\cdot\exp\left[-\frac{\lambda^{o}_{\rho}(s)\,\lambda^{o}_{P}(s)+c^{o}(s)\left(\lambda^{o}_{\rho}(s)+\lambda^{o}_{P}(s)\right)+\tilde{c}^{o}(s)|t|\left(\lambda^{o}_{\rho}(s)+\lambda^{o}_{P}(s)\right)}{\lambda^{o}_{\rho}(s)+4c^{o}(s)+4\tilde{c}^{o}(s)|t|+\lambda^{o}_{P}(s)}|t|\right],$$

and the helicity-flip correlation modified cut:

$$M^{1}_{\rho xP}(\underline{k},s) = \frac{\sqrt{|t|}\,\beta^{1}_{\rho}(s)\beta^{o}_{P}(s)}{4m_{N}\sqrt{\pi}}\exp\left[i\frac{\pi}{2}\left(1-\alpha_{\rho}(o)\right)+i\pi\right]$$

$$\cdot\frac{\lambda^{o}_{P}(s)+2c^{1}(s)+2\tilde{c}^{1}(s)\,|t|}{\left(\lambda^{1}_{\rho}(s)+4c^{1}(s)+\lambda^{o}_{P}(s)+4\tilde{c}^{1}(s)\,|t|\right)^{2}}$$

$$\exp\left[-\frac{\lambda^{1}_{\rho}(s)\,\lambda^{o}_{P}(s)+c^{1}(s)\left(\lambda^{1}_{\rho}(s)+\lambda^{o}_{P}(s)\right)+\tilde{c}^{1}(s)|t|\left(\lambda^{1}_{\rho}(s)+\lambda^{o}_{P}(s)\right)}{\lambda^{1}_{\rho}(s)+4c^{1}(s)+4\tilde{c}^{1}(s)\,|t|+\lambda^{o}_{P}(s)}|t|\right]$$

$$\cdot\left\{\alpha_{\rho}(o)-\frac{2\alpha'_{\rho}}{\lambda^{1}(s)+4c^{1}(s)+4\tilde{c}^{1}(s)\,|t|+\lambda^{o}_{\rho}(s)}\right.$$

$$\left.+\frac{\alpha'_{\rho}\,|t|\left(\lambda^{o}_{p}(s)+2c^{1}(s)+2\tilde{c}^{1}(s)\,|t|\right)^{2}}{\left(\lambda^{1}_{\rho}(s)+4c^{1}(s)+4\tilde{c}^{1}(s)\,|t|+\lambda^{\rho}_{p}(s)\right)^{2}}\right\}.$$

III. Discussion and Results

Our main attention is directed towards the behavior of the kernel in regard to the zero structure of the helicity-nonflip amplitude. The traditional Reggeized absorption model fails; its helicity-nonflip amplitude rotates counter clockwise. The data demand a clockwise rotation ([3]). Therefore the modified cut should have the strength to switch the zero of Im M^0 such that it occurs before the zero of ReM^0. This is what our correlation accomplishes.

We began a search for a possible link between our correlation and the i-factor model by choosing a complex kernel. We found that this violates the analytic properties of the amplitude. But a combination of a purely real correlation kernel and a conventional Pomeron not only fits the data but is theoretically more satisfactory. We illustrate the parallel (Fig. 5a) and perpendicular (Fig. 5b) components of the helicity nonflip amplitude at 6 GeV/c. The flip amplitude is shown in Figs. 6a, 6b. These components are obtained by rotating the amplitude in the complex plane relative to the phase of the isoscalar nonflip helicity amplitude. The parallel and perpendicular components represent, up to this phase, the imaginary and real components of the amplitude respectively. We compare with the amplitude analysis of (3). Particular care is taken to obtain the correct position of the crossover zero. The observables, i.e., differential cross section and polarization, are shown in Figs. 7a and 7b, respectively. For the set of parameters chosen in Table 1, we achieve comparable stability of the crossover zero and polarization over a wide range of energy (Fig. 7b). The differential cross section shows a fair large s and $|t|$ dependence (Fig. 8). Forward turnover

(Fig. 8a) and dips (Figs, 8b, c) are however filled in too strongly with rising energy. Attempts to settle this problem have been made by Refs. 6 and 7, both of which show a strong energy dependence of the phase. Our emphasis in this paper has been to try to obtain a reasonable polarization structure which would remain stable against wide energy variations. Since no one has yet succeeded in producing an amplitude with the correct phase and energy dependence properties ([8]), we feel that the approach of Refs. 6 and 7 could be combined with ours to achieve precisely this. This would automatically be included in Gribov's expansion if the couplings are chosen to be non-planar.

IV. Conclusion

Our findings support our assumption that multiple scattering possesses azimuthal correlations. Once the mutual orientation of the transverse momenta of the Reggeons and Pomeron has been taken into account, phase effects of the data such as polarization are well described. This can be calculated from a fundamental theory—the Reggeon Calculus. The vertices of the theory have to be parameterized more generally than usual so as to include inelastic intermediate states. This is accomplished with the help of a purely real correlation kernel which is responsible for the improvement in the cut phase. Preliminary investigations into line reversed symmetry breaking of charge and hypercharge reactions using the correlation kernel are encouraging.

([6]) Bipin A. Desai and P. R. Stevens, Phys. Rev. D11, 2449 (1975).
([7]) P. D. B. Collins and A. Fitton, Nucl. Phys. B91, 332 (1975).
([8]) G. P. Farmelo and A. C. Irving, Nucl. Phys. B128, 343 (1977).

ACKNOWLEDGMENT

We wish to thank A. B. Kaidalov for helpful correspondence on this work. One of us, P. K., wishes to thank Professor Sidney Drell for his kind hospitality and the Deutscher Akademischer Austauschdienst for their support through a NATO fellowship.

Table 1

Energy scale s_o	1.00	$(\text{GeV/c})^2$
ρ-parameters $\alpha_\rho(o)$	0.52	
α'_ρ	0.804	$(\text{GeV/c})^{-2}$
$\hat{\beta}^o_\rho$; $\hat{\beta}^1_\rho$	1.90; 30.00	$\frac{(\text{mb})^{\frac{1}{2}}}{\text{GeV/c}}$
$\hat{\lambda}^o_\rho$; $\hat{\lambda}^1_\rho$	5.99; 1.40	$(\text{GeV/c})^{-2}$
Pomeron parameters $\alpha_P(o)$	1.00	
$\alpha'_P(o)$	0.3	$(\text{GeV/c})^{-2}$
$\hat{\beta}^o_P$	6.16	$\frac{(\text{mb})^{\frac{1}{2}}}{\text{GeV/c}}$
λ^o_P	2.95	$(\text{GeV/c})^{-1}$
Cut Parameters c^o_1; c^1_1	-1.32; -0.80	$(\text{GeV/c})^{-2}$
c^o_2; c^1_2	-0.10; 1.25	$(\text{GeV/c})^{-2}$
$\tilde{c}^o_1$; $\tilde{c}^1_1$	0.00; 0.00	
$\tilde{c}^o_2$; $\tilde{c}^1_2$	-0.80; 8.00	

FIGURE CAPTIONS

Fig. 1 Gribov's two-body scattering amplitude.

Fig. 2a Gribov's high-energy approximation of the Mandelstam cut.

Fig. 2b Eikonal.

Fig. 3a Unenhanced part of cut amplitude with non-planar coupling.

Figs. 3b,c Semi-enhanced parts of cut amplitude with non-planar couplings.

Fig. 3d Fully enhanced part of cut amplitude with non-planar coupling.

Fig. 4a Traditional eikonal approximation with elastic intermediate states.

Fig. 4b Quasi-eikonal approximation with shower formation in the intermediate states.

Fig. 5a Parallel component of ρ^0 amplitude at 6 GeV/c.

Fig. 5b Perpendicular component of ρ^0 amplitude at 6 GeV/c.

Fig. 6a Parallel component of ρ^1 amplitude at 6 GeV/c.

Fig. 6b Perpendicular component of ρ^1 amplitude at 6 GeV/c.

Fig. 7a Differential cross section of $\pi^- p \to \pi^0 n$ at 6 GeV/c.

Fig. 7b Polarization of $\pi^- p \to \pi^0 n$ at 6 GeV/c and at 200 GeV/c.

Fig. 8a Differential cross section of $\pi^- p \to \pi^0 n$ at very small t and Fermilab energies.

Figs. 8b,c Differential cross section of $\pi^- p \to \pi^0 n$ at Fermilab energies.

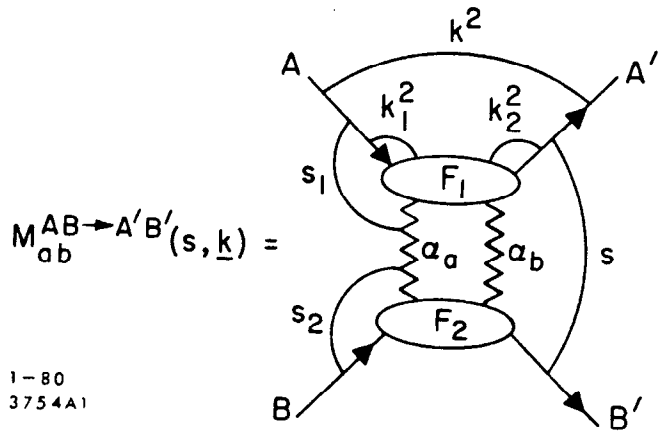
$M_{ab}^{AB\to A'B'}(s,\underline{k})$ =
A
A′
B
B′
k^2
k_1^2
k_2^2
s_1
s_2
s
F_1
F_2
α_a
α_b
1-80
3754A1

Fig. 1

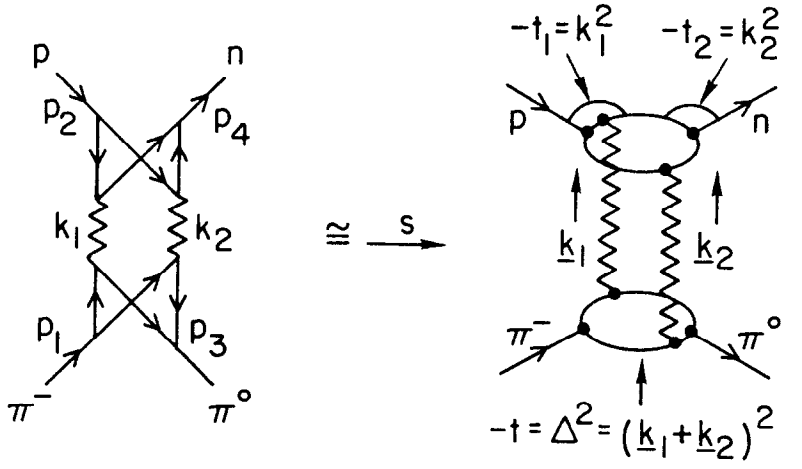

(a)

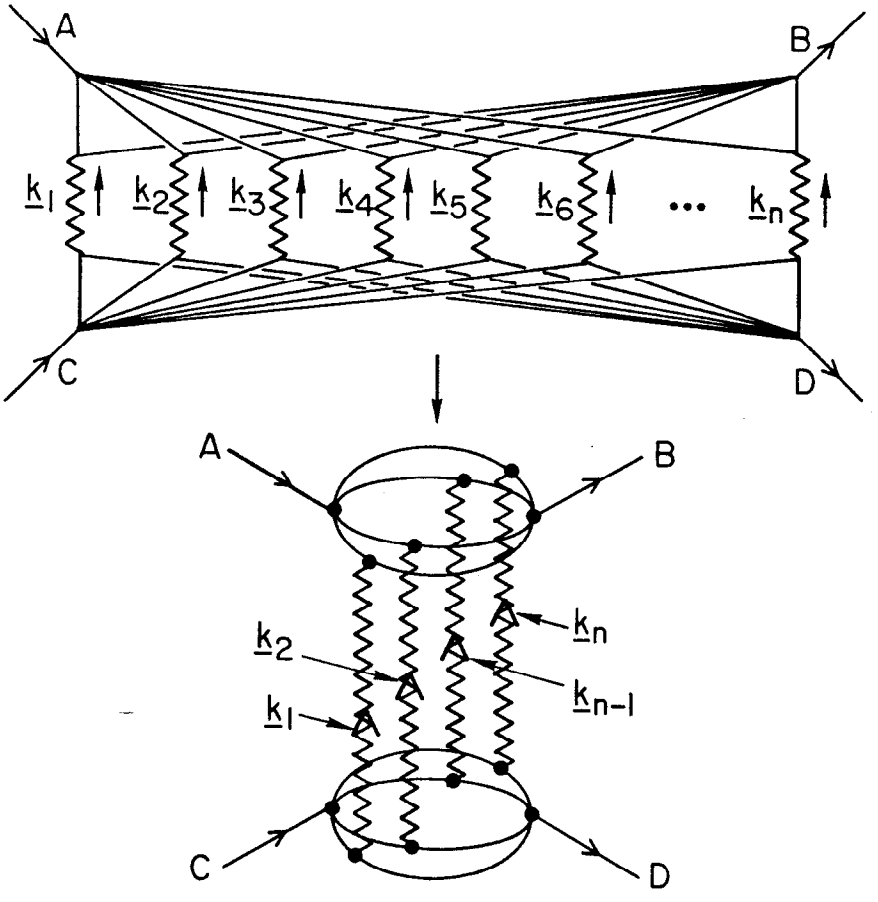

1-80

(b)

3754A2

Fig. 2

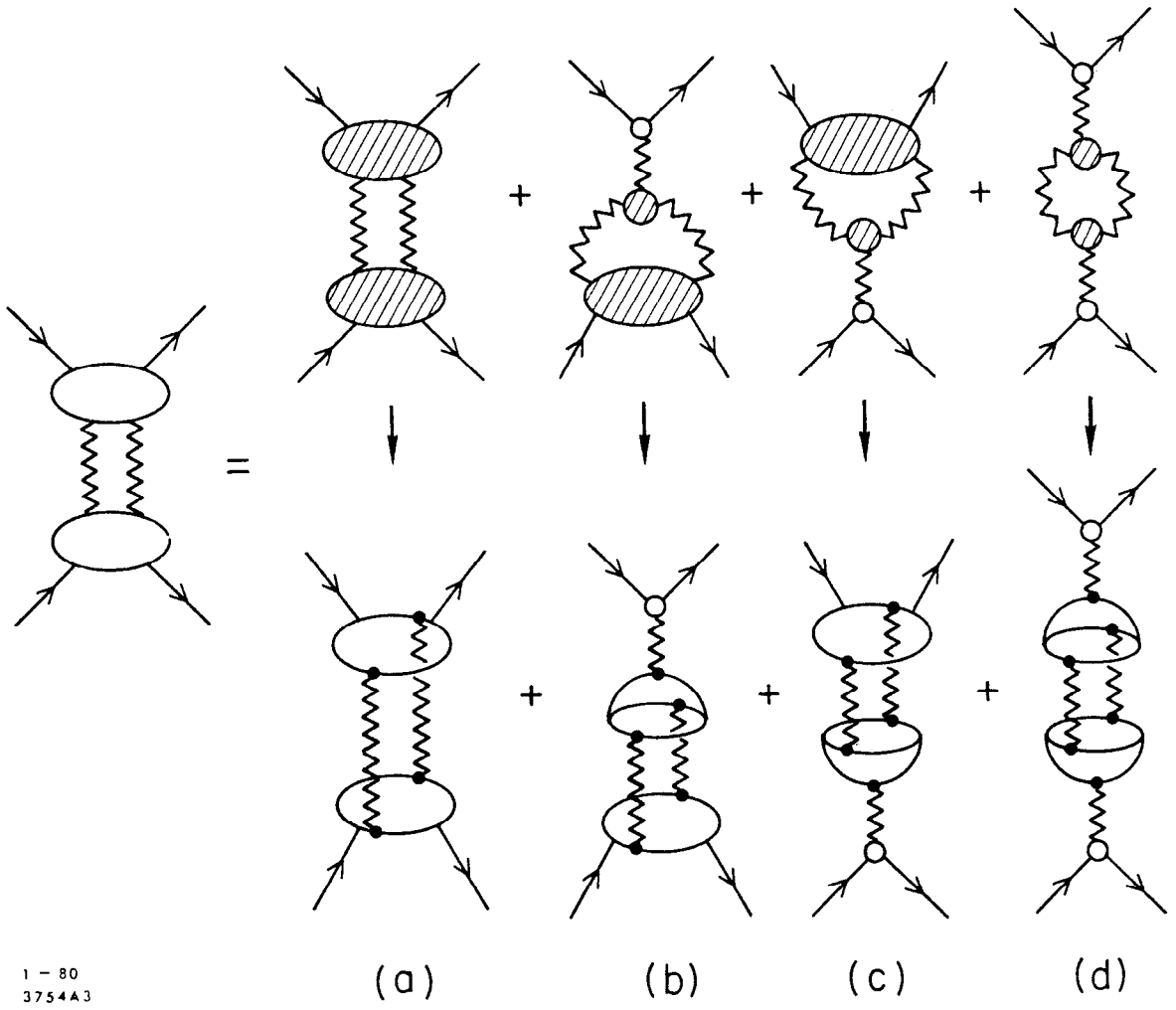

Fig. 3

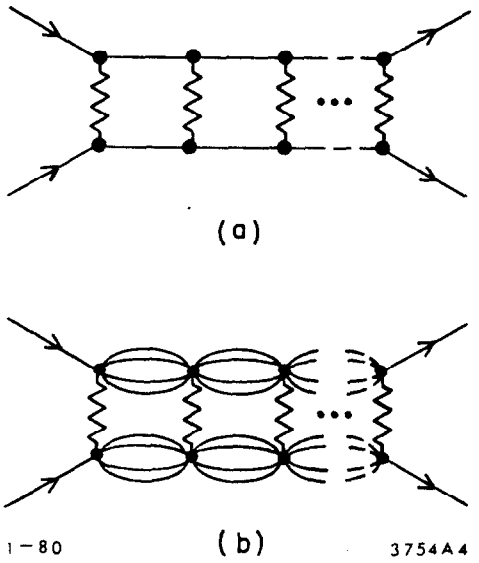

Fig. 4

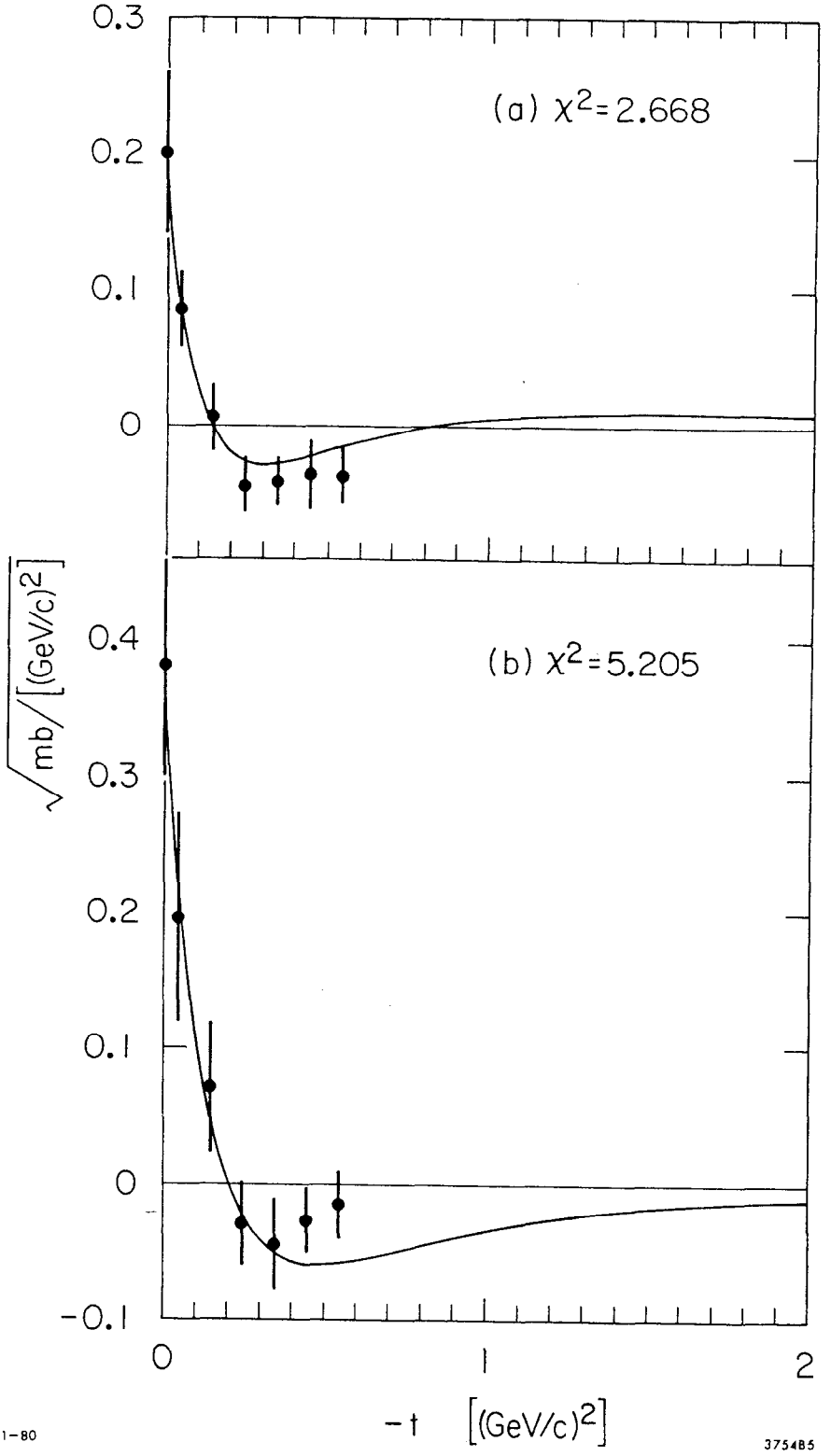
0.3
0.2
0.1
0
(a) χ^2=2.668
0.4
0.3
0.2
0.1
0
-0.1
(b) χ^2=5.205
$\sqrt{mb/[(GeV/c)^2]}$
0
1
2
$-t$ $[(GeV/c)^2]$
1-80
375485

Fig. 5

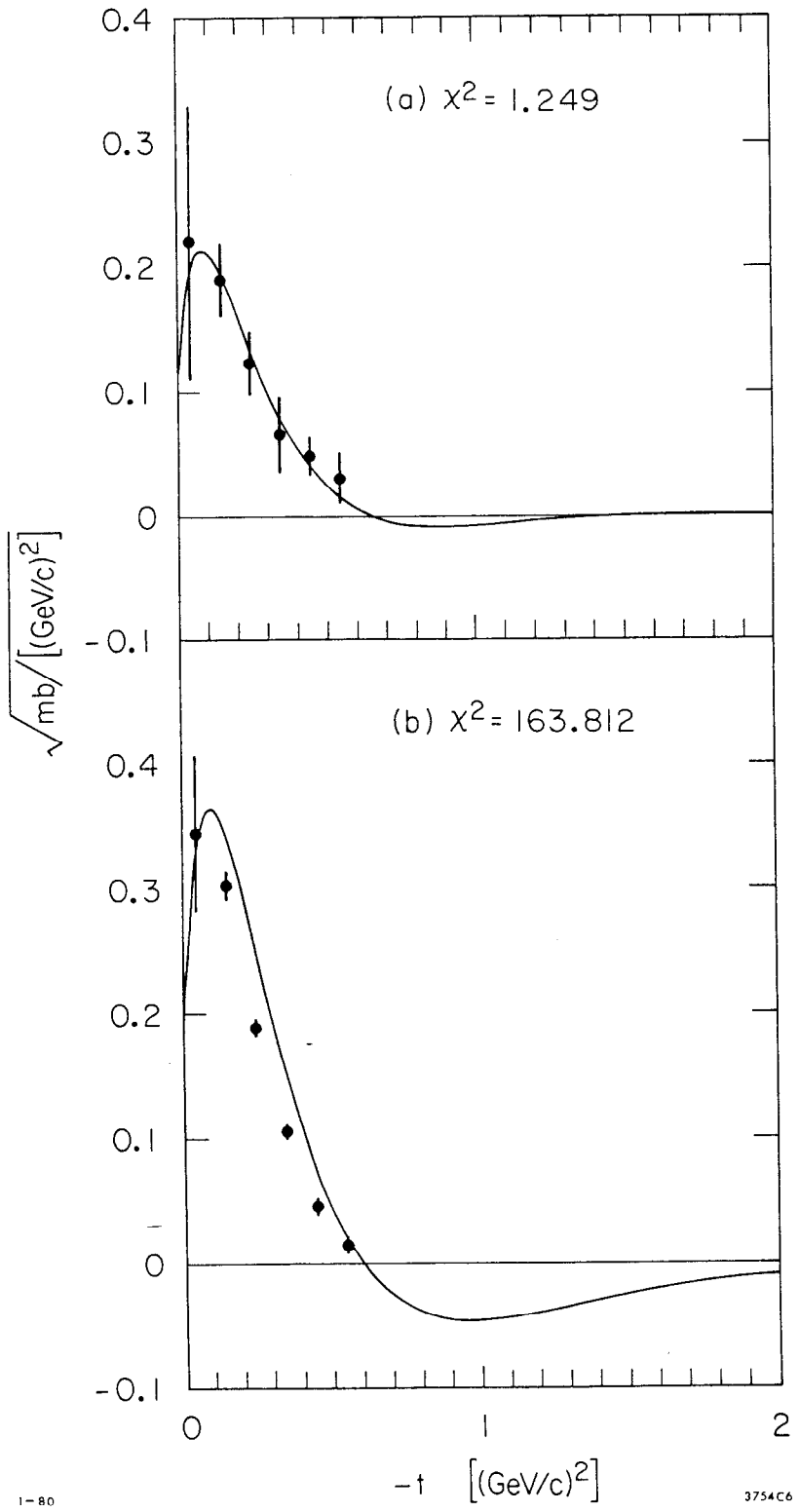
0.4
0.3
0.2
0.1
0
-0.1
(a) $\chi^2 = 1.249$
(b) $\chi^2 = 163.812$
$\sqrt{mb/[(GeV/c)^2]}$
0
1
2
$-t$ $[(GeV/c)^2]$
1-80
3754C6

Fig. 6

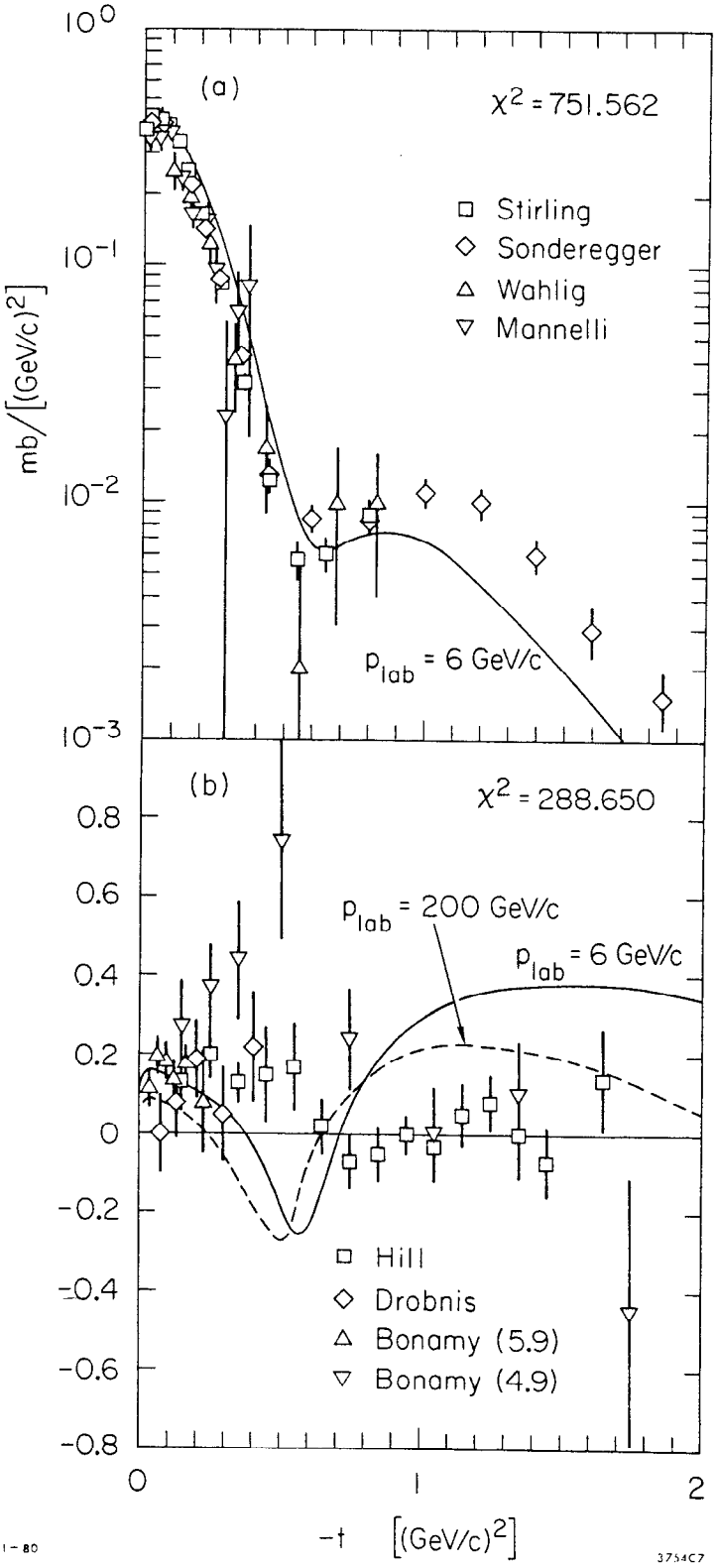
(a)
χ^2 = 751.562
Stirling
Sonderegger
Wahlig
Mannelli
p_{lab} = 6 GeV/c
mb/[(GeV/c)^2]
10^0
10^{-1}
10^{-2}
10^{-3}
(b)
χ^2 = 288.650
p_{lab} = 200 GeV/c
p_{lab} = 6 GeV/c
Hill
Drobnis
Bonamy (5.9)
Bonamy (4.9)
0.8
0.6
0.4
0.2
0
-0.2
-0.4
-0.6
-0.8
0
1
2
-t [(GeV/c)^2]
1-80
3754C7

Fig. 7

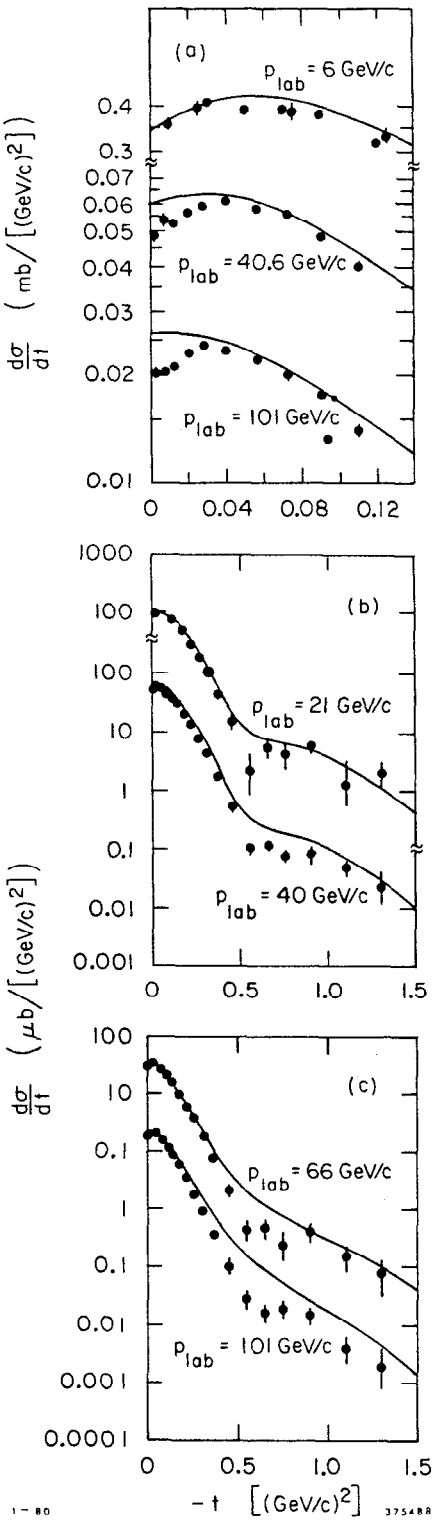
(a)
p_{lab} = 6 GeV/c
p_{lab} = 40.6 GeV/c
p_{lab} = 101 GeV/c
$\frac{d\sigma}{dt}$ (mb/[(GeV/c)^2])
0.4
0.3
0.07
0.06
0.05
0.04
0.03
0.02
0.01
0
0.04
0.08
0.12
(b)
p_{lab} = 21 GeV/c
p_{lab} = 40 GeV/c
$\frac{d\sigma}{dt}$ (μb/[(GeV/c)^2])
1000
100
100
10
1
0.1
0.01
0.001
0
0.5
1.0
1.5
(c)
p_{lab} = 66 GeV/c
p_{lab} = 101 GeV/c
100
10
0.1
1
0.1
0.01
0.001
0.0001
0
0.5
1.0
1.5
$-t$ [(GeV/c)^2]
1-80
375488

Fig. 8